CHEMISTRY OF MATERIALS

ARTICLE

pubs.acs.org/cm

Spongelike Nanosized Mn_3O_4 as a High-Capacity Anode Material for Rechargeable Lithium Batteries

Jie Gao, Michael A. Lowe, and Héctor D. Abruña*

Department of Chemistry and Chemical Biology, Cornell University, Ithaca, New York 14853-1301, United States

ABSTRACT: Mn_3O_4 has been investigated as a high-capacity anode material for rechargeable lithium ion batteries. Spongelike nanosized Mn_3O_4 was synthesized by a simple precipitation method and characterized by powder X-ray diffraction, Raman scattering and scanning electron microscopy. Its electrochemical performance, as an anode material, was evaluated by galvanostatic discharge−charge tests. The results indicate that this novel type of nanosized Mn_3O_4 exhibits a high initial reversible capacity (869 mA h/g) and significantly enhanced first Coulomb efficiency with a stabilized reversible capacity of around 800 mA h/g after over 40 charge/discharge cycles.

KEYWORDS: Mn_3O_4, anode material, lithium batteries, high capacity, Raman scattering

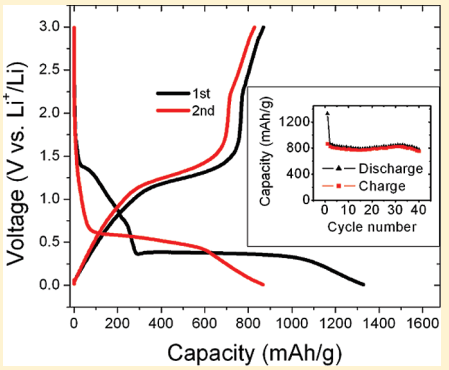

1. INTRODUCTION

Rechargeable lithium ion batteries have revolutionized portable electronic devices. They are also increasingly being pursued for pure electric and hybrid electric vehicle applications. For anode materials, graphite dominates the market for lithium ion batteries because of its moderate capacity, superior cycling performance, and low cost.[1] However, if the battery is overcharged or charged at a high rate, graphite presents safety concerns because of possible lithium plating and/or formation of highly reactive lithium dendrites.[1−4] Furthermore, the practical capacity of graphite is very close to its theoretical value (372 mA h/g) so it is unlikely that additional research will yield significant increases in its capacity. Numerous research groups have been exploring alternative materials with higher capacities and better safety performance. Starting with the report by Tarascon et al. of improved lithium reactivity with metal oxide nanoparticles,[5] several promising nanosized transition-metal oxides have been studied including FeO, NiO, CoO, Co_3O_4,[5] and Fe_3O_4.[6,7] Of particular note, the recent work by Ban et al. on Fe_3O_4 represents a significant advance,[7b] although as is the case for virtually all conversion reactions, they observe a significant irreversible capacity loss after the first cycle (likely associated with the conversion reaction itself) and a significant voltage hysteresis. It is generally believed that these metal oxides react with lithium by a conversion reaction to form lithium oxide and metal nanoparticles: $MO + 2Li^+ + 2e^- = Li_2O + M^0$.[5,8,9] The multielectron reaction results in much higher capacities than graphite, while the more positive reaction potentials for metal oxides (vs Li^+/Li) effectively preclude formation of metallic lithium. However, the dramatic chemical and structural changes that take place during the conversion reaction, suggest that nanoparticle size and shape will play key roles in reaction reversibility.

Although many reports have emphasized the use of cobalt oxide as a promising anode material,[5,10−17] there are relatively few reports on manganese-based anodes. Manganese is less toxic, more abundant in natural resources, and available through current production. At the time of submission, bulk manganese is ∼20 times less expensive than cobalt. Therefore, it is of great interest to further explore manganese-based anode materials.

Surprisingly, previous reports of Mn_3O_4 have suggested that the material has poor lithiation activity, despite being isostructural with Co_3O_4. In one report, pure Mn_3O_4 was shown to have a reversible capacity of just 200 mA h/g, whereas a cobalt-doped sample of Mn_3O_4 exhibited a stable reversible capacity of 400 mA h/g with a first Coulomb efficiency of 45%.[18] Other researchers have prepared Mn_3O_4 nanofibers by electrospinning a polymethylmethacrylate gel with manganese salts and observed a first discharge capacity of 2200 mAh/g with a corresponding charge capacity of only about 580 mAh/g,[19] resulting in a very low first Coulomb efficiency (∼26%). Very recently, a Mn_3O_4/RGO (reduced graphene oxide) composite was reported to exhibit a capacity near its theoretical value.[20]

In this paper, we have synthesized nanosized Mn_3O_4 via a simple precipitation method and evaluated its electrochemical performance as an anode for lithium ion batteries. We also used powder X-ray diffraction, Raman scattering and scanning electron microscopy (SEM) to characterize the structure and morphology of Mn_3O_4. The results indicate that this type of Mn_3O_4 exhibits a high initial reversible capacity (869 mA h/g) and significantly enhanced first Coulomb efficiency with a stabilized reversible capacity of around 800 mA h/g after 40 charge/discharge cycles.

2. EXPERIMENTAL SECTION

Nanosized Mn_3O_4 was synthesized by a simple precipitation method. $Mn(OOCCH_3)_2 \cdot 4H_2O$ was first dissolved in deionized water. The solution was heated to 100 °C in an oil bath. The required amount of

Received: April 12, 2011
Published: June 13, 2011

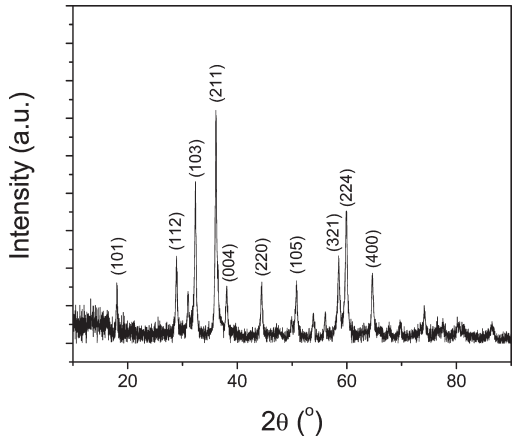

Figure 1. X-ray diffraction pattern of as-prepared Mn_3O_4.

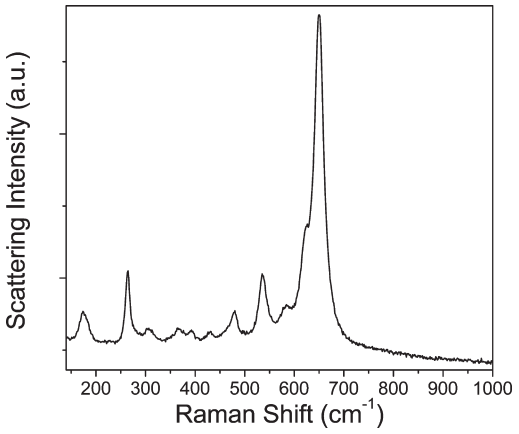

Figure 2. Raman Spectrum from synthesized Mn_3O_4 nanoparticles, showing peaks of both crystalline Mn_3O_4 and amorphous Mn_xO_y.

ammonium hydroxide was subsequently added to the solution. The resulting precipitate was centrifuged after ~4 h of stirring, washed with deionized water, and dried at 80 °C overnight. The nanosized Mn_3O_4 was formed after heating the dried precipitate at 300 °C for 5 h.

Powder X-ray diffraction, employing a Rigaku Ultima IV X-ray Diffractometer operating at 40 kV and 44 mA, using a Cu kα target, was used to characterize the structure of the synthesized sample.

Raman scattering was collected using a Renishaw InVia microRaman system in a backscattering geometry with 785 nm incident radiation. Although previous workers have reported Mn_3O_4 to be stable upon irradiation,[21] care was taken to minimize laser exposure to the sample.

Scanning electron microscopy (SEM), employing a Zeiss 1550 field emission scanning electron microscope, was used to determine the morphology and average particle size of the synthesized Mn_3O_4 powder.

Electrochemical measurements were conducted in CR2032 coin cells. The Mn_3O_4 electrode film was prepared with 70 wt.% Mn_3O_4 as the active material, 20 wt.% Super P−Li (Timcal Ltd.) as a conductive additive, and 10 wt.% poly(vinylidene difluoride) (PVDF) as a binder. N-methyl-2-pyrrolidone (NMP) was used as the solvent to make slurry. The slurry was uniformly coated onto a copper foil current collector with a doctor blade. It was cut into circular electrodes of 0.71 cm^2 area and dried overnight under vacuum at 100 °C. Coin cells were assembled in an argon-filled glovebox with lithium foil as the anode, Celgard 2320 as the separator, and a solution of 1.0 M $LiPF_6$ in ethylene carbonate (EC)/diethyl carbonate (DEC) (1:1 by volume) as the electrolyte. Galvanostatic discharge−charge tests were carried out on Maccor 4000 battery test system. The cells were cycled between 3−0.01 V with different current densities for both discharge and charge processes.

3. RESULTS AND DISCUSSION

The as-prepared Mn_3O_4 powder was first characterized by X-ray diffraction to identify its structure and the diffraction is presented in Figure 1. All peaks could be indexed to Mn_3O_4 as a tetragonal spinel with space group I41/amd (JCPDS card: 24−0734). No other crystalline phases were observed. From the width of diffraction peaks and using the Scherrer equation, we estimate a domain size of around 30 nm.

Raman scattering probes the vibrational modes of both crystalline and amorphous materials, providing complementary structural information to diffraction. Figure 2 shows the Raman spectrum from the synthesized Mn_3O_4 powder. Minor peaks at 308, 364, 475, 581, and a dominant peak at 651 cm^{-1} match reported spectra for crystalline Mn_3O_4.[21,22] In addition, distinct peaks at 173, 263, 535, and 622 cm^{-1} were also observed, likely indicating the presence of an amorphous phase in the sample. These peaks are all in excellent agreement with the reported Raman spectrum for Mn_5O_8 powders obtained by thermal annealing of Mn_3O_4 in air, and which contained a mix of crystalline Mn_5O_8 and Mn_3O_4.[23] Apparently, the dominant peak intensity of Mn_3O_4 is much higher than that of Mn_5O_8. However, no crystalline Mn_5O_8 was observed in the X-ray diffraction. One reason could be from the low content of Mn_5O_8 in the sample. The other reason may be from the lower temperature used in our synthesis procedure that may not have been sufficient to enable formation of the comparatively low symmetry Mn_5O_8 crystal (monoclinic, C1 symmetry).[24] However, the presence of structural elements from Mn_5O_8 is sufficient to explain the Raman spectrum. The similarity between the scattering from Mn_3O_4 and Mn_5O_8 is interesting and indicative of the common structural features of the two compounds.

Figure 3 presents the SEM images of the as-prepared Mn_3O_4 sample. At low magnification (Figure 3. a), it exhibits a sponge-like texture. At high magnification (Figure 3. b), it can be easily seen that the "sponge" block consists of nanosized Mn_3O_4 particles. The average size is about 80 nm. The difference between the domain size estimated by diffraction and electron microscopy would suggest that smaller crystalline domains are joined by amorphous manganese oxide.

Figure 4 shows the first and second discharge−charge profiles of the synthesized Mn_3O_4 at a current rate of 30 mA/g (~0.25 C; 1 C is defined as one lithium per formula in one hour; in the present case, this would represent 117 mA/g for Mn_3O_4) in 1.0 M $LiPF_6$ EC/DEC (1:1 by volume). The general features of the discharge−charge profiles are consistent with other transition metal-oxide anodes that undergo conversion reactions,[5] especially other manganese oxides.[19,25,26] During the first discharge, a sloping voltage is seen from 1.5 to 0.38 V. This may result from concomitant solid-electrolyte interface (SEI) film formation and initial reduction of the metal oxide. Approximately 2 electrons per formula unit are passed during this phase, consistent with reduction of Mn_3O_4 to MnO. However, a slope with only about 1/3 capacity over this voltage range was observed with MnO anodes,[26] indicating that a large fraction of the slope is due to the initial reduction of Mn_3O_4. The main reaction of lithium and Mn_3O_4 is seen in a well-defined voltage plateau around 0.38 V that extends to approximately 1050 mA h/g, slightly more than the theoretical capacity of 937 mA h/g for the conversion

dx.doi.org/10.1021/cm201039w |Chem. Mater. 2011, 23, 3223–3227

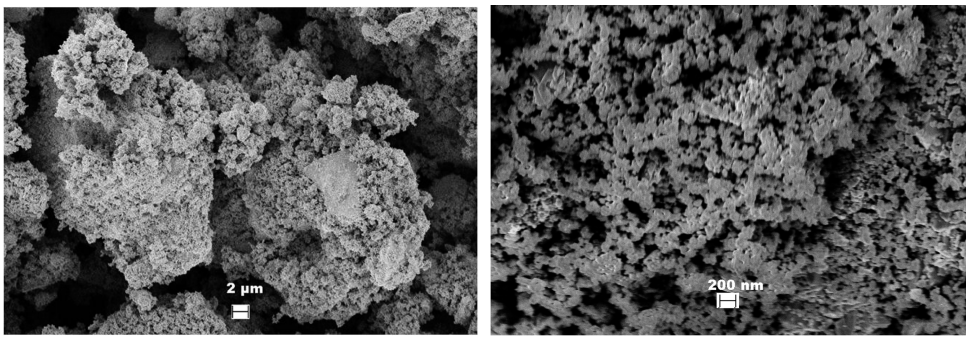

Figure 3. SEM images of the as-prepared Mn_3O_4: (a) low magnification, (b) high magnification.

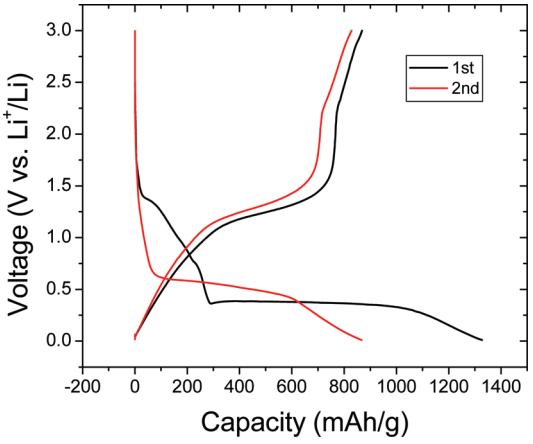

Figure 4. First and second discharge−charge profiles of Mn_3O_4 at a current rate of 0.25 C (1 C is defined as one lithium per formula in one hour, i.e., 117 mA/g for Mn_3O_4) in 1.0 M $LiPF_6$ EC/DEC (1:1 by volume).

reaction to Mn and Li_2O. The overall discharge capacity reaches 1327 mA h/g, with the over discharge capacity approximately consistent with the sloping voltage below 0.37 V.

The first charge curve shows a well-defined voltage plateau around 1.3 V, which is more pronounced and at significantly lower voltage than that of cobalt or iron-based metal oxides,[26] including Co_3O_4.[16] Approximately 6 electrons per formula unit of initial Mn_3O_4 are removed by the end of this plateau, consistent with oxidation of each Mn to MnO. An additional shoulder is observed when the material is charged above 2 V, which was not seen for MnO.[26] This may correspond to further oxidation of MnO to Mn_3O_4. The first charge capacity approaches 869 mA h/g, which is very close to the theoretical capacity of a fully reversible conversion reaction (e.g., oxidation to Mn_3O_4). This value is comparable to the reported reversible capacity of Co_3O_4 and is much higher than the capacity of commonly used graphitic carbon. Interestingly, the value we obtain is also much higher than bare Mn_3O_4 without RGO which only exhibited capacities below 300 mA h/g.[20] This could result from the different preparation method that we developed, which gives rise to a different morphology. Although we also observed a significant irreversible capacity loss after the first cycle, such behavior is common to virtually all systems based on conversion reactions.

As has been reported for a number of transition metal oxides, the second discharge profile is different from the first one. Only one voltage plateau was observed around 0.6 V, which was distinctly higher and more sloped than the main feature of the first discharge. This may indicate that the lithiation reaction of the second cycle is easier and is often the feature of a single phase reaction. The investigation of the specific reaction mechanism is currently under way via in situ X-ray techniques including X-ray diffraction and X-ray absorption spectroscopy. It is worth noting that the second charge profile is very similar to the first charge. This means that the electrochemical reaction becomes highly reversible after the first discharge, which is consistent with its good cycling performance as discussed below. Although there is still a voltage hysteresis between discharge and charge, due to the nature of a conversion reaction, the hysteresis is less than that observed for other conversion systems like Co_3O_4[16] or Fe_3O_4.[7b]

Figure 5 presents the changes in discharge−charge capacity and Coulomb efficiency of Mn_3O_4 with cycling at a rate of 0.25 C. It can be seen that the cycling is quite stable. The reversible capacity exhibits almost no significant fading after 40 cycles. In addition, the Coulomb efficiency reaches more than 65% for the first cycle, much higher than previous reports on Mn_3O_4[18,19] and as good as carbon-coated MnO nanoparticles.[26] It remains at over 95% during all subsequent cycles.

The rate capability of our Mn_3O_4, which is important for practical applications, was also evaluated. Figure 6 shows representative discharge−charge profiles of Mn_3O_4 at current rates of 0.25 C, 2.5 and 10 C. At 2.5 C, the reversible capacity reaches about 640 mA h/g. Even at 10 C, the material can deliver a capacity close to 500 mA h/g. Such a high current rate performance also is a very attractive feature of our system, which could be further improved by the use of conductive additives and/or modifiers.

The outstanding electrochemical performance of the synthesized Mn_3O_4 could be attributed to its special architecture. The nanoscale provides large surface area, which improves the utilization of active material, and the loose porous sponge structure allows lithium ions to transfer easily in and out. The material is also able to accommodate the strain induced by possible volume change during discharge−charge process and maintain the integrity of the electrode. This may be responsible for the good cycling stability.

While several different manganese oxides have been proposed for lithium battery anodes, all exhibit very similar behavior. This may indicate that (i) it is the nature of the metal that determines

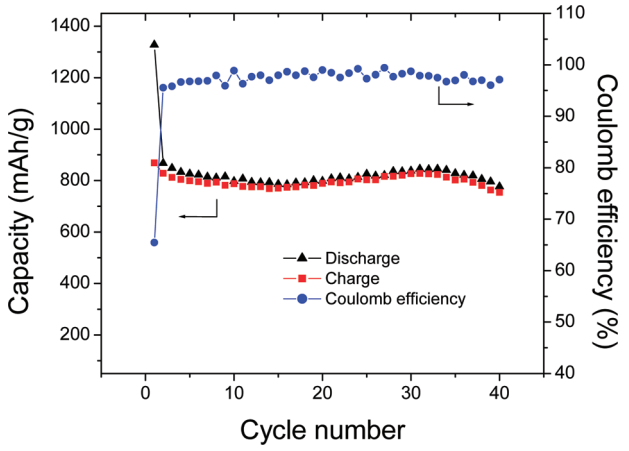

Figure 5. Cycle performance and Coulomb efficiency of Mn_3O_4 at a current rate of 0.25 C in 1.0 M $LiPF_6$ EC/DEC (1:1 by volume).

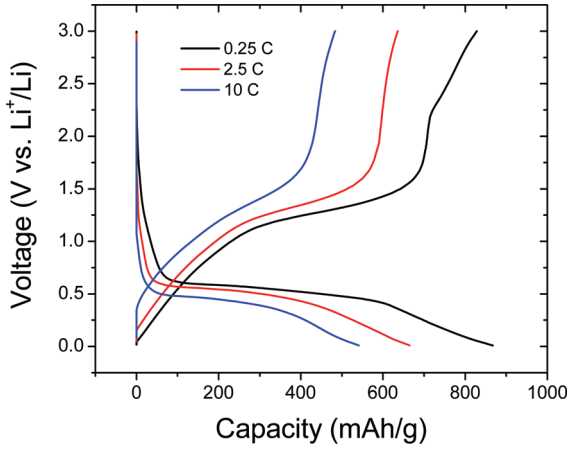

Figure 6. Representative discharge−charge profiles of Mn_3O_4 at current rates of 0.25, 2.5, and 10 C in 1.0 M $LiPF_6$ EC/DEC (1:1 by volume).

the voltage plateaus; (ii) nanoparticle morphology and starting crystal structure are the key factors for stable cycling performance.

Mn_3O_4 possesses lower operating voltages (peak potentials of ~1.3 V on oxidation and 0.6 V on reduction) compared to Co_3O_4 (2.1 V on oxidation, 1.2 V on reduction).[18] When combined with a specific cathode, the full cell operating voltage will be higher and so will the energy density. In the meantime, the lithiation voltage of Mn_3O_4 (~0.6 V) is higher than that of typical graphitic carbon (below 0.2 V). This feature facilitates the exclusion of possible lithium plating and consequently results in much better safety performance. The synthesis process of Mn_3O_4 is also very simple with no need for expensive chemicals nor special equipment or processing. Manganese is environmentally benign, much more abundant and inexpensive than cobalt. Notably, we have not optimized the synthesis process and cell configuration, and clearly enhanced electrochemical performance would be anticipated with optimization. All of the above advantages as well as its high capacity make Mn_3O_4 a very attractive candidate as an anode material for the next generation of rechargeable lithium ion batteries.

4. CONCLUSIONS

Spongelike nanosized Mn_3O_4 anode material for rechargeable lithium batteries has been synthesized by a very simple precipitation method. The X-ray diffraction pattern shows no crystalline impurities in the as-synthesized sample. Raman scattering indicates the presence of low content of amorphous Mn_5O_8. SEM images show that the average particle size is about 80 nm. Electrochemical measurements indicate that the special nanosized Mn_3O_4 shows a high initial reversible capacity (869 mA h/g) and a stabilized reversible capacity of around 800 mAh/g upon cycling. The electrochemical reaction becomes highly reversible after the first discharge, and the reversible capacity exhibits almost no significant fading after 40 cycles. The Coulomb efficiency for the first cycle reaches more than 65% and remains at over 95% during the subsequent cycles. The outstanding electrochemical performance of this specific Mn_3O_4 could be attributed to its special architecture.

AUTHOR INFORMATION

Corresponding Author

*Tel.: +1 607 255 4720. Fax: +1 607 255 9864. E-mail: hda1@cornell.edu.

ACKNOWLEDGMENT

This work is supported by the Energy Materials Center at Cornell (EMC2), an Energy Frontier Research Center funded by the U.S. Department of Energy, Office of Science, Office of Basic Energy Sciences under Award Number DE-SC0001086. Some battery testing was performed using resources at the KAUST-Cornell Center for Energy and Sustainability (KAUST-CU). MAL gratefully acknowledges funding from a National Defense Science and Engineering Graduate fellowship. The authors also acknowledge use of the Keck SEM administered by the NSF -MRSEC at Cornell.

REFERENCES

(1) Tarascon, J.-M.; Armand, M. *Nature* **2001**, *414*, 359–367.
(2) Verbrugge, M. W.; Koch, B. J. *J. Electroanal. Chem.* **1997**, *436*, 1–7.
(3) Arora, P.; Doyle, M.; White, R. E. *J. Electrochem. Soc.* **1999**, *146*, 3543–3553.
(4) Goodenough, J. B.; Kim, Y. *Chem. Mater.* **2010**, *22*, 587–603.
(5) Poizot, P.; Laruelle, S.; Grugeon, S.; Dupont, L.; Tarascon, J.-M. *Nature* **2000**, *407*, 496–499.
(6) Taberna, P. L.; Mitra, S.; Poizot, P.; Simon, P.; Tarascon, J.-M. *Nat. Mater.* **2006**, *5*, 567–573.
(7) (a) Zhang, W.-M.; Wu, X.-L.; Hu, J.-S.; Guo, Y.-G.; Wan, L.-J. *Adv. Funct. Mater.* **2008**, *18*, 3941–3946. (b) Ban, C.; Wu, Z.; Gillaspie, D. T.; Chen, L.; Yan, Y.; Blackburn, J. L.; Dillon, A. C. *Adv. Mater.* **2010**, *22*, E145–E149.
(8) Bruce, P. G.; Scrosati, B.; Tarascon, J.-M. *Angew. Chem., Int. Ed.* **2008**, *47*, 2930–2946.
(9) Armand, M.; Tarascon, J.-M. *Nature* **2008**, *451*, 652–657.
(10) Larcher, D.; Sudant, G.; Leriche, J.-B.; Chabre, Y.; Tarascon, J.-M. *J. Electrochem. Soc.* **2002**, *149*, A234–A241.
(11) Kang, Y.-M.; Kim, K.-T.; Kim, J.-H.; Kim, H.-S.; Lee, P. S.; Lee, J.-Y.; Liu, H. K.; Dou, S. X. *J. Power Sources* **2004**, *133*, 252–259.
(12) Li, W.-Y.; Xu, L.-N.; Chen, J. *Adv. Funct. Mater.* **2005**, *15*, 851–857.
(13) Nam, Ki. T.; Kim, D.-W.; Yoo, P. J.; Chiang, C.-Y.; Meethong, N.; Hammond, P. T.; Chiang, Y.-M.; Belcher, A. M. *Science* **2006**, *312*, 885–888.

(14) Du, N.; Zhang, H.; Chen, B.; Wu, J.; Ma, X.; Liu, Z.; Zhang, Y.; Yang, D.; Huang, X.; Tu, J. *Adv. Mater.* **2007**, *19*, 4505–4509.
(15) Li, Y.; Tan, B.; Wu, Y. *Nano Lett.* **2008**, *8*, 265–270.
(16) Lou, X. W.; Deng, D.; Lee, J. Y.; Feng, J.; Archer, L. A. *Adv. Mater.* **2008**, *20*, 258–262.
(17) Lu, Y.; Wang, Y.; Zou, Y.; Jiao, Z.; Zhao, B.; He, Y.; Wu, M. *Electrochem. Commun.* **2010**, *12*, 101–105.
(18) Pasero, D.; Reeves, N.; West, A. R. *J. Power Sources* **2005**, *141*, 156–158.
(19) Fan, Q.; Whittingham, M. S. *Electrochem. Solid-State Lett.* **2007**, *10*, A48–A51.
(20) Wang, H.; Cui, L.; Yang, Y.; Casalongue, H. S.; Robinson, J. T.; Liang, Y.; Cui, Y.; Dai, H. *J. Am. Chem. Soc.* **2010**, *132*, 13978–13980.
(21) Bernard, M.-C.; Hugot-Le Goff, A.; Thi, B. V.; Cordoba de Torresi, S. *J. Electrochem. Soc.* **1993**, *140*, 3065–3071.
(22) Julien, C. M.; Massot, M.; Poinsignon, C. *Spectrochim. Acta A* **2004**, *60*, 689–700.
(23) Azzoni, C. B.; Mozzati, M. C.; Galinetto, P.; Paleari, A.; Massarotti, V.; Capsoni, D.; Bini, M. *Solid State Commun.* **1999**, *112*, 375–378.
(24) Oswald, H. R.; Wampetich, M. J. *Helv. Chim. Acta* **1967**, *50*, 2023–2034.
(25) Zhao, J.; Tao, Z.; Liang, J.; Chen, J. *Cryst. Growth Des.* **2008**, *8*, 2799–2805.
(26) Zhong, K.; Xia, X.; Zhang, B.; Li, H.; Wang, Z.; Chen, L. *J. Power Sources* **2010**, *195*, 3300–3308.